Nuclear Materials and Energy 12 (2017) 506–512

Contents lists available at ScienceDirect

Nuclear Materials and Energy

journal homepage: www.elsevier.com/locate/nme

Plasma impact on diagnostic mirrors in JET

A. Garcia-Carrasco[a,*], P. Petersson[a], M. Rubel[a], A. Widdowson[b], E. Fortuna-Zalesna[c], S. Jachmich[d], M. Brix[b], L. Marot[e], JET Contributors[1]

[a] Royal Institute of Technology (KTH), SE-10044 Stockholm, Sweden
[b] EUROfusion Consortium, JET, Culham Science Centre, Abingdon, OX14 3DB, UK
[c] Faculty of Materials Science and Engineering, Warsaw University of Technology, 02-507 Warsaw, Poland
[d] Laboratory for Plasma Physics, Ecole Royale Militaire-Koninklijke Militaire School, 1000 Brussels, Belgium
[e] Department of Physics, University of Basel, Klingelbergstrasse 82, CH-4056 Basel, Switzerland

ARTICLE INFO

Article history:
Received 29 June 2016
Revised 29 November 2016
Accepted 27 December 2016
Available online 16 February 2017

Keywords:
JET
First mirror test
Diagnostic mirrors
Erosion-deposition

ABSTRACT

Metallic mirrors will be essential components of all optical systems for plasma diagnosis in ITER. This contribution provides a comprehensive account on plasma impact on diagnostic mirrors in JET with the ITER-Like Wall. Specimens from the First Mirror Test and the lithium-beam diagnostic have been studied by spectrophotometry, ion beam analysis and electron microscopy. Test mirrors made of molybdenum were retrieved from the main chamber and the divertor after exposure to the 2013–2014 experimental campaign. In the main chamber, only mirrors located at the entrance of the carrier lost reflectivity (Be deposition), while those located deeper in the carrier were only slightly affected. The performance of mirrors in the JET divertor was strongly degraded by deposition of beryllium, tungsten and other species. Mirrors from the lithium-beam diagnostic have been studied for the first time. Gold coatings were severely damaged by intense arcing. As a consequence, material mixing of the gold layer with the stainless steel substrate occurred. Total reflectivity dropped from over 90% to less than 60%, i.e. to the level typical for stainless steel.

1. Introduction

In ITER, optical diagnostics will rely on metallic mirrors, known as “first mirrors”, to access plasma while maintaining neutron shielding. Optical stability of first mirrors will be essential to ensure reliability of diagnostics [1]. First mirrors will undergo modification due to plasma-wall interaction (PWI) processes. Erosion by impinging particles will change roughness and chemical composition of material by co-implantation. Deposition of plasma impurities together with fuel species will lead to the formation of coating layers on the surface of mirrors. Both situations will result in the degradation of reflectivity. There is an ongoing research in fusion experiments to assess the performance of first mirrors and to elaborate solutions to prolong their lifetime. Some examples are the works at JET [2], TEXTOR [3], DIII-D [4], Tore Supra [5] and HL-2A [6]. Also, laboratory experiments on simulation of neutron-induced effects are carried out to assess the impact of transmutation, material damage and helium production on optical properties of mirrors [7,8].

The aim of this contribution is to provide a comprehensive account on the modification of diagnostic mirrors by PWI processes in JET with the ITER-Like Wall (ILW) [9]. Two different types of mirrors have been studied: specimens from the First Mirror Test (FMT) [10-12] and, for the first time, mirrors from the lithium-beam diagnostic.

The FMT project is realised for ITER with the aim to determine plasma impact on the optical performance of diagnostic mirrors. The project started in 2001 on the request of the ITER Design Team. The FMT research program involves: (i) selection of material for mirrors, (ii) production of mirrors and their carriers for in-vessel installation, (iii) optical pre-characterization, (iv) exposure in different locations in JET (main chamber and divertor) during an entire operational campaign, and (v) comprehensive post-mortem analyses by means of surface-sensitive techniques to assess optical properties and morphology. Until now, complete sets of results have been obtained after two experimental campaigns in JET-C, i.e. with carbon walls [10,11] and after the first experimental campaign

* Corresponding author.
E-mail address: alvarogc@kth.se (A. Garcia-Carrasco).

[1] See the Appendix of F. Romanelli et al., Proceedings of the 25th IAEA Fusion Energy Conference 2014, Saint Petersburg, Russia.

http://dx.doi.org/10.1016/j.nme.2016.12.032

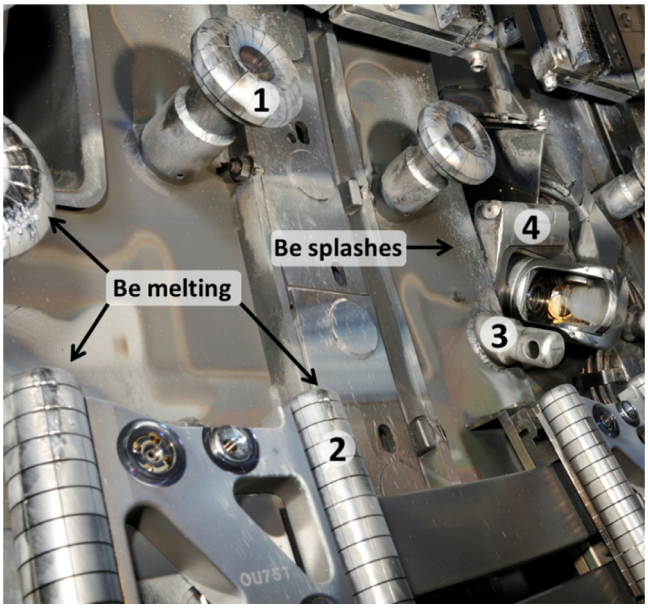

Fig. 1. Top of the JET vessel: 1,2) beryllium limiters, 3) crane rail, 4) periscope head with Li-beam diagnostic mirror.

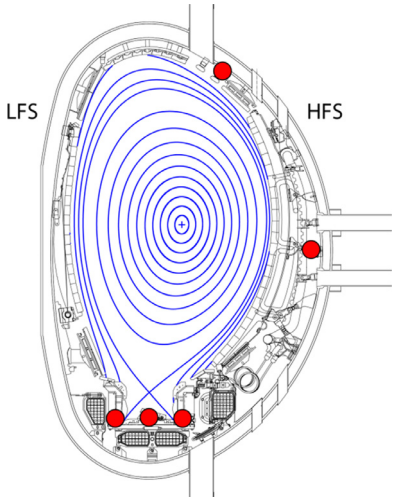

Fig. 2. Cross-section of JET. Test mirrors are located in the outer mid-plane and in the divertor area. The Li-beam diagnostic mirror is located in the top of the vessel. (For interpretation of the references to colour in the text, the reader is referred to the web version of this article.)

(2011–2012) in JET-ILW [12]. This work concentrates on mirrors exposed during the second ILW campaign in 2013–2014.

The purpose of the lithium-beam diagnostic system at JET is to measure electron density profiles at the plasma edge. It is based on the injection of a neutral lithium beam with energies of 20–70 kV and the subsequent analysis of photon-emission profiles produced by the interaction of lithium with plasma electrons. Because a wide variety of plasma shapes are explored at JET, it is necessary to use a mirror with an adjustable tilt angle to detect light from a given region of interest at the plasma edge [13]. It should be stressed that these are the first-ever material studies on actual diagnostic mirrors from JET.

2. Experimental

2.1. Mirrors

Twenty test mirrors were retrieved from JET-ILW after the 2013–2014 experimental campaign. All mirrors were made of polycrystalline molybdenum with a surface area of $1 \times 1\,cm^2$. Some surfaces were additionally coated using magnetron sputtering with a 1 μm thick layer of molybdenum or rhodium [14,15]. Test mirrors were installed in stainless steel carriers placed in the outer mid-plane of the main chamber wall and in the divertor: outer and inner leg and below the base tile. The carriers had channels in which mirrors could be mounted at different depths, thus having different solid angles with respect to the plasma. The information about the carriers and their installation in the JET vessel is detailed in [2].

The Li-beam diagnostic mirrors were retrieved after the 2011–2012 and 2013–2014 experimental campaigns. The mirrors were $13 \times 5\,cm^2$ and 1 cm thick plates made of bulk stainless steel with a gold coating. They were installed in a periscope head on top of the vessel at about 42 cm from plasma. Fig. 1 shows the top of JET vessel with the Li-beam diagnostic mirror in the periscope head surrounded by various types of limiters, e.g. castellated mushroom roof limiters. The location in the JET vessel of all studied mirrors is marked in red in Fig. 2.

The total plasma exposure time during the 2013–2014 campaign was 19.5 h (13.5 h in divertor configuration) and the total energy input was 201 GJ. The injected deuterium was 2×10^{26} atoms and the injected nitrogen as extrinsic radiator was 2×10^{24} atoms. Table 1 presents a comparison of parameters between the first and second ILW campaigns. When comparing to ITER, the entire 2013–2014 campaign corresponds in terms of time to 122 ITER discharges (400 s, Q = 10) but only to 4 ITER discharges scaled by energy input and about 1 ITER discharged in terms of divertor fluence [16].

Table 1
Comparison of parameters between the first (2011–2012) and second (2013–2014) campaigns at JET-ILW.

	2011–2012	2013–2014
Total plasma time (h)	18.9	19.5
Divertor plasma time (h)	13.1	13.5
Input energy (GJ)	151	201
Injected D (10^{23} atoms)	1165	1826
Injected N (10^{23} atoms)	5	19

2.2. Analysis methods

The most important property of a mirror is light reflectance. Total and diffuse reflectivity of mirrors was measured in the visible and near infra-red range (400–1600 nm). Surface and near-surface composition of mirrors was examined using several complementary accelerator-based methods at the Tandem Accelerator Laboratory (Uppsala University, Sweden). Deuterium and beryllium concentrations were measured by nuclear reaction analysis (NRA) with a 2.8 MeV $^3He^+$ beam. This method cannot be used to measure carbon in beryllium contaminated samples because protons produced from the nuclear reactions $^{12}C(^3He, p)^4He$ and $^9Be(^3He,p)^{11}B$ have similar energies and the resulting energy spectrum cannot be resolved. Tungsten concentration was measured using Rutherford backscattering spectrometry (RBS), also with a 2.8 MeV $^3He^+$ beam. The thickness of the gold coating of the Li-beam diagnostic mirrors was measured by RBS using a 3 MeV proton beam. Concentration of light species (Be, C, N and O) was measured by time-of-flight heavy ion elastic recoil detection analysis (ToF-ERDA) with a 36 MeV $^{127}I^{8+}$ beam. This method is suited to determine composition depth profiles because of excellent mass separation between light elements and good depth resolution of a few nm [17]. The main disadvantage is the sensitivity to surface roughness because

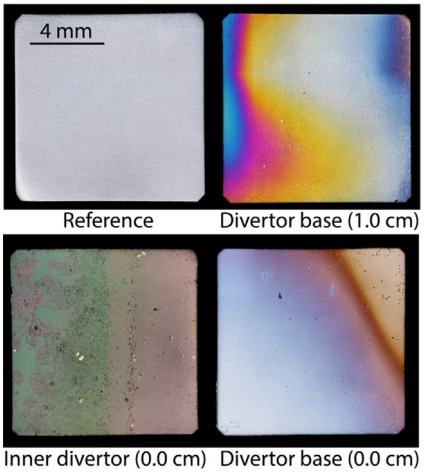

Fig. 3. Visual inspection of divertor mirrors after exposure to plasma.

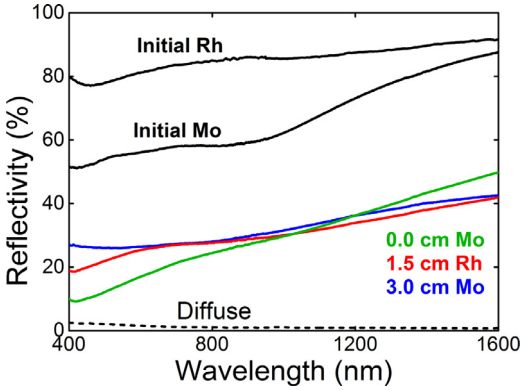

Fig. 4. Reflectivity of outer divertor mirrors before and after exposure to plasma. The distances 0.0, 1.5, 3.0 cm refer to the depth of the mirror in the channel of the carrier. The solid and dashed lines correspond to total and diffuse reflectivity respectively.

of low incidence angle (22°). However, this is not an issue in the analysis of mirrors.

The morphology and composition of mirror surfaces was studied also by means of optical and scanning electron microscopy (SEM) using Hitachi SU8000 (beam energy 0.5–30 keV) combined with energy-dispersive X-ray spectroscopy (EDS Thermo Scientific Ultra Dry, type SDD – silicon drift detector) and YAG BSE (backscattered electrons) detector. The EDS system is capable of beryllium detection and quantification, as shown earlier in studies of dust specimens from the JET divertor [18].

3. Results

3.1. First mirror test

3.1.1. Mirrors from the divertor

Visual inspection revealed that all divertor mirrors were covered with smooth-looking layers displaying a variety of colourful patterns thus indicating inhomogeneous material deposition. The appearance of several surfaces is presented in Fig. 3. The total reflectivity was degraded by 50–80% regardless of the substrate material or the location in the carrier. The plot in Fig. 4 shows the reflectivity for the outer divertor mirrors before and after the exposure to plasma. The distances in the legend refer to the depth of the mirror in the channel of the carrier. The solid and dashed lines correspond to total and diffuse reflectivity respectively. Diffuse reflectivity was very similar for all mirrors (below 5%) and only one trace is shown in the figure as a reference.

Table 2
Composition of deposits of divertor mirrors. All numbers are in units of 10^{15} cm^{-2}.

	Inner	Base	Outer
D	70–1391	69–245	23–680
Be	175–3602	353–670	325–4850
C	6–(>431)	14–29	17–72
N	19–(>434)	29–96	31–248
O	111–(>1950)	304–652	226–1484
W	2–114	4–12	4–19

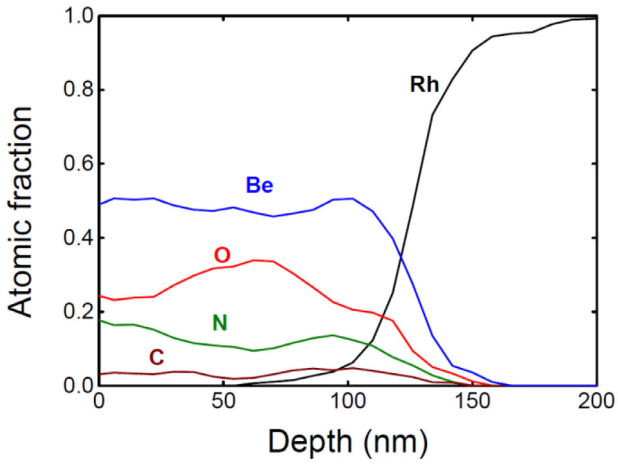

Fig. 5. Concentration depth profile of rhodium mirror located in the inner divertor, 1.5 cm deep into the channel of the carrier.

Surface composition of divertor mirrors is presented in Table 2. The main impurity is beryllium, followed by oxygen, nitrogen, deuterium, carbon, tungsten and traces of Inconel constituents (Ni, Cr, Fe); the latter is not shown in the table. The total thickness of deposits is in the range from 50 nm to 1 µm. Such layer thickness completely blocks the light from reaching the mirror substrate. This explains why reflectivity of all mirrors is degraded to a similar level regardless of the position and the substrate (Mo or Rh). The reflected signal originates from the deposit itself. As a reference, the intensity of light falls when penetrating Mo and Be with an exponential decay length of 13 and 15 nm respectively at 600 nm [19,20].

Impurity concentrations are similar to those measured on the mirrors exposed to the 2011–2012 experimental campaign [12] with the exception of carbon, whose levels are significantly lower, approximately by a factor of 5. The main reason is that during the 2011–2012 experimental campaign, mirrors were installed in-vessel right after changing from the carbon to the metal first wall. During the initial operation phase in 2011, carbon concentration in plasma was decreasing to values approximately 15 times smaller than measured in JET with carbon wall and this lower level remained during the remaining part of the campaign [21]. That tendency was also perfectly reflected by HIERDA measurements on mirrors from the first ILW campaign [12]. It is also stressed that low carbon levels have been measured in 2013–2014 operation [22]. The increased use of nitrogen as extrinsic radiator in the second campaign might have also contributed to the lower carbon deposition by the so-called scavenging effect [23]. An example of concentration depth profiles is shown in Fig. 5. It is recorded for a rhodium-coated mirror from the inner divertor placed 1.5 cm into the channel of the carrier. Traces for only some impurity species (Be, O, C, N) are shown for clarity of the figure. The thickness

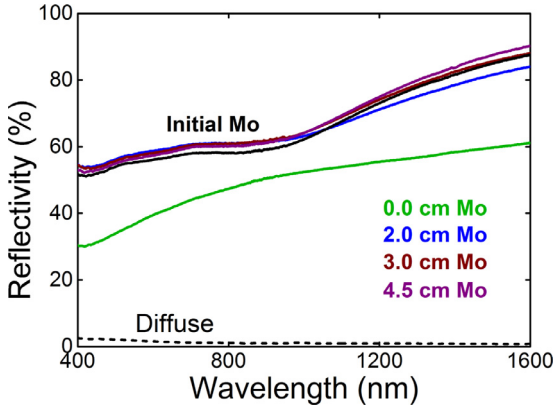

Fig. 6. Reflectivity of main chamber mirrors before and after exposure to plasma. The distances 0.0, 2.0, 3.0, 4.5 cm refer to the depth of the mirror in the channel of the carrier. The solid and dashed lines correspond to total and diffuse reflectivity respectively.

Table 3
Composition of deposits of main chamber mirrors. The distances 0 cm and 1.5–4.5 cm indicate depth into the channel of the carrier. All numbers are in units of 10^{15} cm^{-2}.

	0 cm	1.5–4.5 cm
D	390	3–20
Be	7300	0–5
C	30	20–30
N	94	0–5
O	1125	1–20
W	2	0

of the deposit is approximately 100 nm. It is composed mainly of beryllium and oxygen. The increase of oxygen at a depth of 50 nm is most probably associated with the in-vessel intervention (and venting the torus) to retrieve a broken reciprocating probe. The measured fluctuation of the oxygen content in deposits reflects the machine operation history. One may tentatively state that the oxygen detected in the co-deposit is associated with in-vessel processes (co-deposition of O impurity species) and not with the oxidation of the entire layer once mirrors were removed from the torus.

3.1.2. Mirrors from the main chamber

The reflectivity plots for the mirrors from the main chamber are shown in Fig. 6. The solid and dashed lines correspond to total and diffuse reflectivity respectively. Diffuse reflectivity was very similar for all mirrors (below 5%) and only one trace is shown in the figure as a reference. There is a decrease in total reflectivity by about 20% for the specimen located at the entrance of the carrier. However, total reflectivity of all other mirrors is maintained or even slightly increased in the visible range as a result of erosion of Mo oxides by impinging neutral particles, as discussed in more detail in [12].

Surface composition of the mirrors is presented in Table 3. There is a significant difference between the specimen at the carrier entrance and those located deeper. In the latter case the concentrations of D, Be, C, N and O impurities are at the level of about $1–3 \times 10^{16}$ cm^{-2}, while tungsten is below the detection limit of 5×10^{13} cm^{-2}. On the contrary, the mirror at the entrance (position 0 cm) is coated by a layer of 600 nm composed mainly of beryllium. Photographic survey performed during the shut-down showed melting of beryllium limiters in the vicinity of the mirror carrier. The fairly thick beryllium layer was most probably formed during such off-normal events, including the damage to limiters

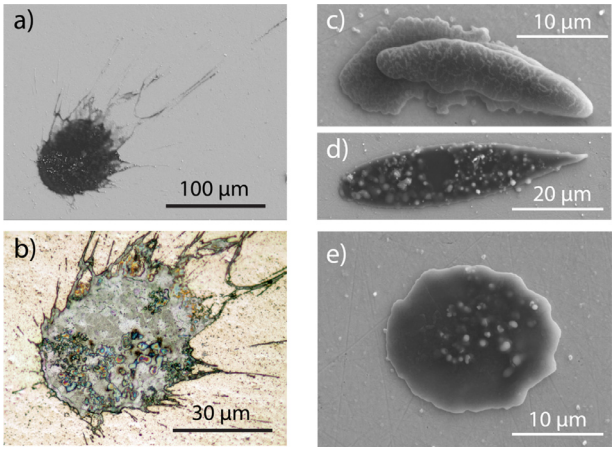

Fig. 7. Images of beryllium splashes on the surface of the mirror at position 0 cm. The splashes have elongated (a-d) or flat (e) shapes. Images (a) and (b) show the same particle under electron and optical microscopy respectively.

(especially upper dump plate) caused by run-away electrons in experiments performed at the very end of the campaign.

Results of detailed topographical studies performed with SEM and EDS on the mirror at position 0 cm are shown in Figs. 7 and 8. On top of the fairly uniform co-deposits there are numerous macroscopic particles of various shape and size: from 3 μm to over 100 μm. These are elongated splashes (Fig. 7 (a–d)), flat splashes (Fig. 7(e)) and spherical droplets (Fig. 8(a)). The variety of objects gives strong indication that they were deposited at different events. The splashes cannot be associated with a single disruption because they have different orientations. A common feature of all these objects is the presence of beryllium as the main component. The other detected elements in all particles are: C, N, O and traces of steel and Inconel alloy constituents. The spherical droplet shown in Fig. 8(a) is not splashed and its composition is complex (see EDS spectrum in Fig. 8(b)). Besides light elements there are also heavy species: W, Mo, Ni, Cu and Fe. This gives a fairly strong indication that the origin of such particle(s) is not associated with melting and splashing of the limiter material. One may suggest that it is most probably a W-Mo or W-Ni particle formed earlier in another region of the machine and then transported, for instance, during a disruption.

3.2. Li-beam diagnostic mirrors

Li-beam diagnostic mirrors were retrieved after the 2011–2012 and 2013–2014 campaigns. Images in Fig. 9 show the appearance of those mirrors. In both cases, significant areas of their surfaces were damaged. The topography of the damaged area, as recorded by optical microscopy in Fig. 10, clearly proves melting of the surface layer (Au coating and the stainless steel substrate) by arcing. Arcing is a well-known erosion process in fusion devices [24-28]. The main conditions to form electric arcs are a sufficiently high potential and an electron-emission spot such as a small surface protrusion (for instance, a beryllium droplet). In the presence of magnetic fields, the cathode spot moves across the material in the direction perpendicular to the magnetic field. This effect is known as retrograde motion and it produces characteristic dendrite-like tracks, as those observed in the mirror [29].

Total and diffuse reflectivity plots in the visible and near infrared range are presented in Fig. 11. The initial values were measured on a spare twin mirror because the decision to study the mirror was taken after plasma exposure to determine the cause of the damage in the surface. Total reflectivity decreased after plasma exposure from over 90% to about 60%. The values after plasma

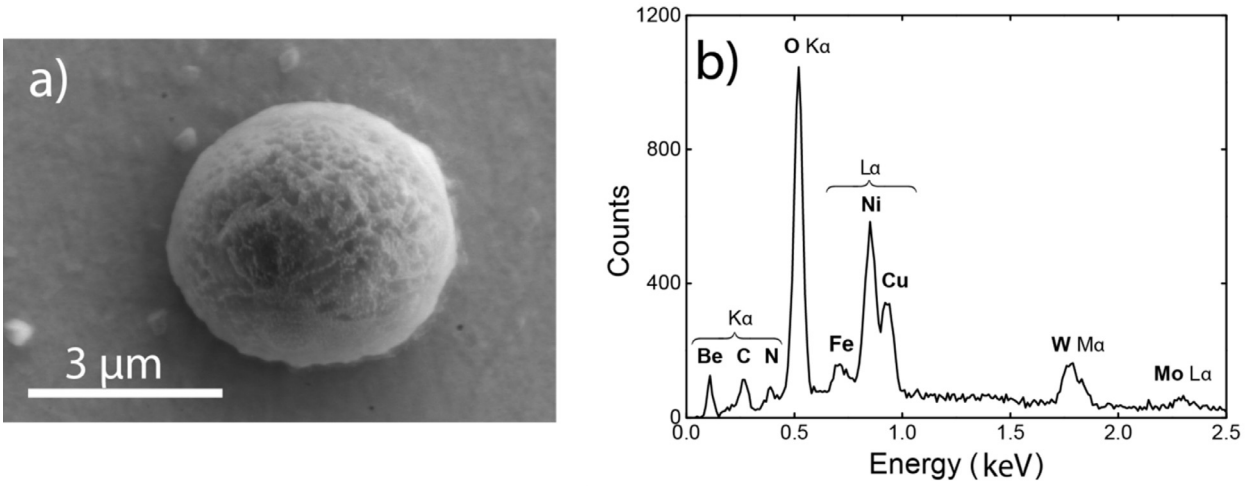

Fig. 8. (a) Spherical droplet on the surface of the mirror at position 0 cm, (b) EDS spectrum of the spherical droplet.

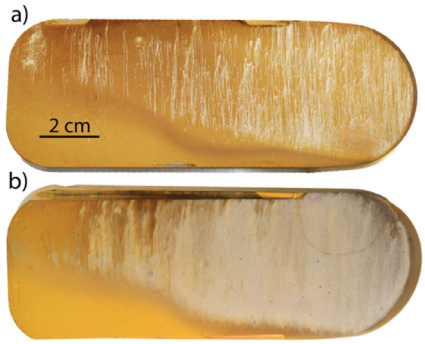

Fig. 9. Li-beam diagnostic mirrors after exposure in JET in a) 2011–2012 experimental campaign, b) 2013–2014 experimental campaign.

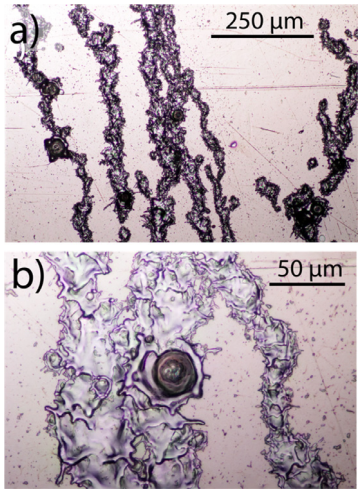

Fig. 10. Optical microscopy pictures of the surface of the Li-beam diagnostic mirror: a) arc traces along the mirror surface, b) detail of material melting produced by arcing.

exposure resemble those characteristics for stainless steel. This suggests erosion of the gold layer and consequent mixing with stainless steel in the surface region. In the visible range, diffuse reflectivity increased from 2% to more than 15% as a result of surface roughening by arcing. In conclusion, optical properties of the mirror were significantly degraded.

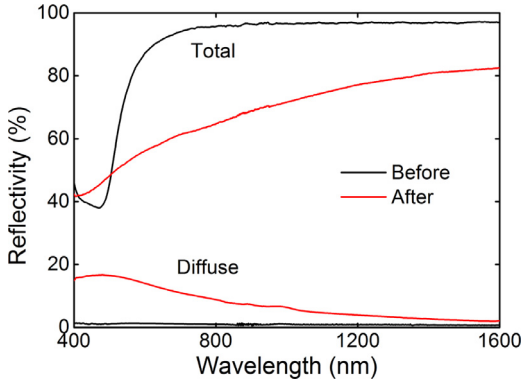

Fig. 11. Total and diffuse reflectivity of the Li-beam diagnostic mirror before and after exposure to plasma during the 2013–2014 campaign. (For interpretation of the references to colour in the text, the reader is referred to the web version of this article.)

The result of analysis with RBS for the mirror exposed during 2013–2014 is presented in Fig. 12. Initially, there was a well-defined gold layer of 0.6 μm on top of a stainless steel substrate. After exposure, the gold signal is reduced and overlaps with the stainless steel background. This indicates a reduction in the gold concentration by a factor of 2 (from 3.7 to 1.8×10^{18} cm^{-2}) and strong material mixing being a result of melting. In the damaged area, the concentrations of D and Be were up to 5×10^{17} cm^{-2} and 10×10^{17} cm^{-2}, respectively. The origin of these impurities is probably splashing of the melt layer from nearby beryllium limiters (see Fig. 1). The splashed beryllium could act as a hot spot for the initiation of electric arcs. The other possibility for creating the first protrusion was a local detachment of the Au coating. In addition, the impact of so-called "parasitic plasma" due to local electric fields in the periscope system cannot be excluded, though it is difficult to prove; no direct measurement can be performed. The concept of such discharges in narrow spaces was proposed [30-32]. In the non-damaged area, the concentrations of D and Be were much lower (about 1×10^{16} cm^{-2}) because of the protection given by the crane rail placed in front of the periscope head.

4. Concluding remarks

There are several important contributions of this work to the determination of plasma impact on the mirror performance and

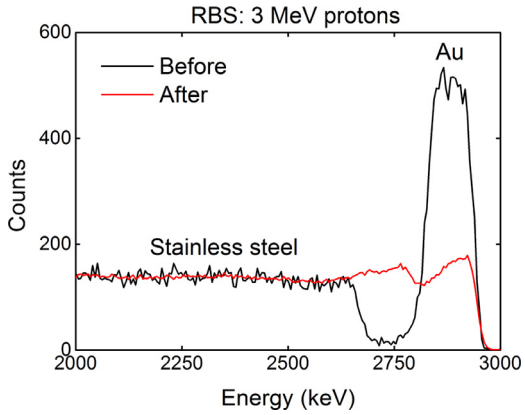

Fig. 12. RBS spectrum of the Li-beam diagnostic mirror before and after exposure to plasma during the 2013–2014 campaign.

on material erosion and transport in the main vessel and in the divertor. Studies performed with a set of complementary material analysis techniques clearly show beryllium splashes and fine metal (W, Ni) droplets deposition on mirror surfaces in the main chamber. This has never been observed at earlier stages of FMT, neither in JET-C nor in JET-ILW. Mirrors in the divertor are coated with multi-layer deposits containing both W and Be [33], thus proving transport of metals to shadowed regions. Mirrors, with their smooth surfaces can be considered as perfect deposition monitors. This type of probes with mirror-finish surfaces can serve in ITER as long-term samples to assess material migration [34]. Using ToF-ERDA depth profiling, one can then "deconvolute" the operation history. It should be stressed that all specimens, both in the main chamber and in the divertor, contained nitrogen which was originally puffed only in the divertor region. Nitrogen levels are fairly constant over the entire operation period. Carbon content in mirrors is about 5 times lower in the second campaign with respect to the first campaign. Detection of only traces of carbon on surfaces provides a positive message regarding the stability of W coatings on tiles made of carbon fibre composites (CFC).

Degradation of reflectivity by deposition of beryllium and other impurities on the mirrors exposed in the main chamber has been effectively reduced by placing the mirrors deeper in the channels. This experimental fact has had an impact on the ongoing design of reactor diagnostics. A dedicated mirror holder of has been developed in the ITER – JET cooperation and it was installed on the main chamber wall of JET [35]. In the divertor area, reflectivity of all mirrors has been significantly degraded regardless of the substrate material or the position in the channel. In ITER, the situation will might be even worse due to the upscale in material migration as a consequence of higher input energies and plasma exposure time. These results highlight the need of techniques to mitigate reflectivity degradation of mirrors. Photonic methods are considered to remove co-deposits. However, this approach requires beforehand knowledge of the composition and thickness of the co-deposits to set up laser parameters in order to avoid surface damage. Photonic methods were tested on JET mirrors with beryllium-containing deposits and they did not provide satisfactory results [36-38]. The use of replaceable protective filters is also ruled out because they would be promptly degraded by gamma and neutron irradiation. Methods based on radio frequency plasma generated locally close to the mirrors are under development, but early results indicate the increase of diffuse reflectivity of the cleaned surfaces of mirrors from JET [39]. The best results so far have been obtained by mechanical cleaning [40]. It should be stressed that all above mentioned works [36-40] were carried out ex-situ, i.e. on mirrors retrieved from JET and then comprehensively characterised after the exposure. Baffled channels with a series of fins are being tested to reduce impurity deposition on mirrors; results from JET-ILW are still under evaluation. Other solutions point to the use of shutters to limit plasma exposure time. Cassettes with replaceable mirrors are also considered for the divertor region where deposition effects may very strongly reduce the reliability of measurements.

For the first time, surface analyses have been performed on a diagnostic mirror from JET. Part of the surface of the Li-beam diagnostic mirror was severely damaged by intense arcing. The gold coating layer and the stainless steel substrate of the mirror had been melted, changing completely its optical properties. The most probably reason for arc initiation is splashing of molten material from the surrounding limiters. This idea is supported by the significantly higher amount of deposits found in the area affected by arcing with respect to the non-damaged area, which was protected from impurity deposition by a crane rail structure placed in front of the periscope head.

These results contribute to the discussion on the applicability of coated mirrors and they also strongly point to the need of very careful selection of mirrors locations, including the surrounding, and the design of diagnostic channels. The ongoing test of the dedicated mirror holder in the main chamber [35] is expected to provide further indications for the design process. In summary, the studies of mirrors have had an impact on the development and testing of several schemes for the prolongation of mirrors' lifetime, i.e. cleaning and protection.

Acknowledgements

This work has been carried out within the framework of the EUROfusion Consortium and has received funding from the Euratom research and training programme 2014–2018 under grant agreement No 633053. The views and opinions expressed herein do not necessarily reflect those of the European Commission. The work has been partly funded by the Swedish Research Council (VR) through contracts no. 621-2012-4148 and 2015-04844. We thank the staff of the Tandem Accelerator Laboratory at the Uppsala University for their help during the ion beam analysis measurements. The authors would like to thank Héctor Escorial for his help in the processing of optical microscopy images.

Supplementary materials

Supplementary material associated with this article can be found, in the online version, at doi:10.1016/j.nme.2016.12.032.

References

[1] A.E. Costley, et al., Fusion Eng. Des. 74 (2005) 109.
[2] M. Rubel, et al., Rev. Sci. Instr. 77 (2006) 063501.
[3] P. Wienhold, et al., J. Nucl. Mat. 337 (2005) 1116.
[4] A. Litnovsky, et al., Fusion Eng. Des. 83 (2008) 79.
[5] M. Lipa, et al., Fusion Eng. Des. 81 (2006) 221.
[6] Y. Zhou, et al., Fusion Eng. Des. 81 (2006) 2823.
[7] A. Garcia-Carrasco, et al., Nucl. Instr. Meth. B 382 (2016) 91.
[8] K. Ono, Phys. Scr. T138 (2009) 014065.
[9] G.F. Matthews, Phys. Scr. T145 (2011) 014001.
[10] M. Rubel, J. Nucl. Mater. 390-391 (2009) 1066.
[11] M. Rubel, et al., Phys. Scr. T145 (2011) 014070.
[12] D. Ivanova, Phys. Scr. T159 (2014) 014011.
[13] M. Brix, et al., Rev. Sci. Instr. 81 (2010) 10D733.
[14] L. Marot, et al., Rev. Sci. Instr. 78 (2007) 103507.
[15] L. Marot, et al., Surf. Coat. Technol. 202 (2008) 2837.
[16] R.A. Pitts, Plasma Phys. Control. Fusion 47 (2005) B300.
[17] P. Ström, et al., Rev. Sci. Instr. 87 (10) (2016) 103303.
[18] A. Baron-Wiechec, et al., Nucl. Fusion 55 (2015) 113033.
[19] M.M. Kirillova, et al., Soviet Physics JETP 33 (1971) 1210.
[20] A.D. Rakić, et al., Appl. Optics 37 (1998) 5271.
[21] S. Brezinsek, J. Nucl. Mater. 438 (2013) S303.
[22] S. Brezinsek, et al., Nucl. Fusion 55 (2015) 063021.

[23] F. Tabares, Plasma Phys. Control. Fusion 46 (2004) B381.
[24] M Rubel, et al., J. Nucl. Mater 307-311 (2002) 111.
[25] M. Laux, J. Nucl. Mater 313-316 (2003) 62.
[26] V. Rhode, J. Nucl. Mat. 438 (2013) S800.
[27] D. Rudakov, J. Nucl. Mat. 438 (2013) S805.
[28] G.F. Federici, et al., Nucl. Fusion 41 (2001) 1967.
[29] B. Jüttner, et al., J. Phys. 33 (2000) 2025.
[30] M. Rubel, J. Nucl. Mater. 283-297 (2000) 1089.
[31] V. Rohde, J. Nucl. Mater. 313-316 (2003).
[32] V. Rohde, Phys. Scr. T103 (2003).
[33] E. Fortuna-Zaleśna, et al., Nucl. Mater. Ener. (2017) http://dx.doi.org/10.1016/j.nme.2016.11.027. in press.
[34] Ph. Mertens, et al., Phys. Scr. T159 (2014) 014004.
[35] Z. Vizvary, et al., Fus. Eng. Des. (2017). http://dx.doi.org/10.1016/j.fusengdes.2016.12.016. in press.
[36] A. Widdowson, J. Nucl. Mater. 415 (2011) S1199.
[37] A. Leontyev, et al., Fusion Eng. Des. 86 (2011) 1728.
[38] M. Wisse, et al., Fusion Eng. Des. 89 (2014) 122.
[39] L. Moser, Phys. Scr. T167 (2016) 014069.
[40] D. Ivanova, J. Nucl. Mater. 438 (2013) S1241.